Interaction of trailing vortices in the wake of a wall-mounted rectangular cylinder

Amalendu Sau,[1] Robert R. Hwang,[1,2,*] Tony W. H. Sheu,[3] and W. C. Yang[1]
[1]*Institute of Physics, Academia Sinica, Taipei-11529, Taiwan*
[2]*Department of System Engineering, National Taiwan Ocean University, Keelung, Taiwan*
[3]*Department of Engineering Science and Ocean Engineering, National Taiwan University, 73 Chou-Shan Rd., Taipei, Taiwan, Republic of China*
(Received 8 April 2003; published 18 November 2003)

Numerical simulations are performed to investigate three-dimensional unsteady vortex-vortex and vortex-surface interactions in the near field of a wall-mounted rectangular cylinder placed inside a channel. The generation mechanism of the upstream and the trailing vortices from the topologically important critical points and their near-wall evolution pattern have been examined in detail. In the upstream region, a laminar necklace vortex system formed around the junction between the rectangular block (cylinder) and the flat channel floor. A sequence of streamwise vortical rollers dominated the downstream interaction region, and they exhibited strong unsteady vortex-surface interaction. Streamwise vortices which formed upstream of the obstacle exhibited quadrupole structure with the dominant pair being central downwash, whereas those lifting the flow behind the obstacle were of predominantly central upwash. Notably, at some downstream location, the near-wall wake structure was observed to locally disappear due to mutual interaction and annihilation by opposite strength vortices on either side of the wake centerline. During the entire course of unsteady flow evolution, such a disappearance of the wake remained closely associated with local contraction of the limiting streamlines on the channel floor, the development of a pair of topologically important floor critical points (saddles), and the presence of a near-wall node on the vertical symmetry plane. The dominance of inward transverse flow toward these saddles together with flow evolution from the downstream node on the vertical symmetry plane were found to be particularly responsible for facilitating the local interaction of various vortices of opposite strength, leading to significant vorticity cancellation in the region. Moreover, the basic source of the wake vortices and their nature of evolution behind the cylinder were also investigated here, and they were found to be fundamentally different from what one usually observes in the near-wake of a transverse jet. However, the growth of a pair of vertically lifting vortices from the spiraling shear layer nodes just behind the downstream edge of the cylinder base was detected in this flow configuration also.

DOI: 10.1103/PhysRevE.68.056303 PACS number(s): 47.15.Ki, 47.27.Vf, 47.32.Cc, 47.32.Ff

I. INTRODUCTION

Understanding the complex three-dimensional unsteady vortex interactions around surface mounted obstacles is a subject of considerable interest. Such flow situations are frequently encountered in our practical life, starting from atmospheric flows and flow over protuberances on aircraft to cooling of computer chips on a circuit board, depending on the shape and size of the obstacle. Upon encountering the adverse pressure hill generated by the presence of the obstacle, there takes place local reversal of the boundary layer fluid, which creates a separation region ahead of the obstacle. The accumulated upstream boundary layer vortices, in the presence of continued spanwise pressure gradient along the lateral sides of the obstacle, form a U-shaped horseshoe vortex system around the body (e.g., Baker [1], Mason and Sykes [2], Hunt and Snyder [3], Thomas [4], and Seal *et al.* [5]), with its two arms extending downstream. The observations made by Baker [1], Thomas [4], and Seal *et al.* [5] further reveal that the developed horseshoe vortex can be steady or unsteady depending on the Reynolds number, the thickness of the boundary layer, and the base width of the body. Even in fully developed turbulent boundary layers such a vortex structure survives (Seal and Smith [6]). Trailing vortices with different senses of orientation (i.e., vortices with positive or negative sign) are a common feature of the wakes behind different surface-mounted obstacles. However, details of the streamwise interaction and the structural evolution of the unsteady near-wall wake vortices behind a wall-mounted obstacle, and particularly the phenomenon of local disappearance of the wake due to vorticity cross cancellation (i.e., due to close interaction between vortices of a particular strength issuing from one side of the cylinder and those of opposite strength issuing from the other side), remain poorly addressed. Previous investigations of the wakes of bodies generating upstream horseshoe vortices indicate the existence of nested pairs of trailing vortices (e.g., Hunt and Snyder [3] and Mason and Morton [7]) of opposite strength in the far wake. The common belief was that the dominant wake vortices which remain present behind the wall-mounted obstacles are the streamwise extension of the two arms of the upstream horseshoe vortices. However, observations made by Mason and Morton [7] suggest that, among the downstream extended streamwise wall vortices seen in the wake, only the outermost vortices are actually the extension of the trailing edges of the upstream horseshoe vortex, and they are relatively weak. The stronger core vortices as observed by them behind a wall-mounted obstacle are con-

*FAX: 886-2-2783-4187. Electronic address: phhwang@ccvax.sinica.edu.tw

sidered to be the product of the inner wake, and the nature of their dynamics is directly influenced by the obstacle shape. The findings of Mason and Morton [7] further revealed that the inner wake behind surface-mounted obstacles consists of pairs of opposite sign streamwise vortices, which display their close interaction with the existing boundary layer vortices and the subsequent complex process of vorticity cross cancellation at a downstream location.

One important consequence of the cross cancellation of streamwise vortices is the local disappearance of the wake. However, until today there exists very little work on the topic, and much less is known about the mechanism leading to the wake disappearance. The phenomenon of vorticity cancellation usually takes place in the near wake of the obstacles. The local acceleration and deceleration of the flow in the wake facilitates the wake disappearance due to vorticity cross cancellation. The physical reason behind the wake disappearance is that in accelerating flows the opposite signed vorticity on each side of the wake, which normally diffuses outward, gets confined and distorted by the mean flow. The process of vorticity cancellation always remains associated with local flow acceleration and convergence of the mean streamlines in the near-wake region. In addition to the analysis and measurements as provided by Keffer [8] and Elliott and Townsend [9] indicating the effect of converging or diverging streamlines on wake disappearance, the recent theoretical work on the topic by Hunt and Eames [10] underscores the need for computing such complex flows to shed further light on the governing physical process.

The control and modification of aerodynamic boundary layers with the help of the dynamics of trailing vortices, as produced by using simple vortex generators, have been addressed by Cook *et al.* [11] and by Jenkins *et al.* [12]. The extended trailing vortices observed in these studies are also seen to originate from the wake and they are not extensions of the upstream vortices. These trailing vortices are particularly effective in providing the necessary lift to aerodynamic bodies. However, the source of inception of the vortices has not been addressed properly. Moreover, here it may be appropriate to mention that vortex generators are also being used for producing suitable streamwise vortices that can effectively enhance mixing in combustion (e.g., Zaman *et al.* [13], Zaman [14], and Sau [15,16]). The vortices originating behind the tabs (small protrusions into the flow) are generated due to uneven flow acceleration as caused by skewing of the local pressure gradient. Formation of unsteady horseshoe vortices upstream of a jet in a cross flow has been observed by Kelso and Smits [17] among others. In a recently conducted DNS study Sau *et al.* [18] investigated the near-field behavior of a jet in a cross flow and observed that the unsteady characteristics of the upstream horseshoe vortex system are directly transmitted into the jet near wake, leading to its asymmetric and unsteady growth. However, none of the far-wake vortices found around the jet in a cross flow were extended tails of the upstream vortices. In fact, they originated from the cross-flow wall boundary layer (e.g., Fric and Roshko [19] and Kelso *et al.* [20]). It is particularly in the context of finding the topological source and investigating the downstream dynamics and interaction of the streamwise

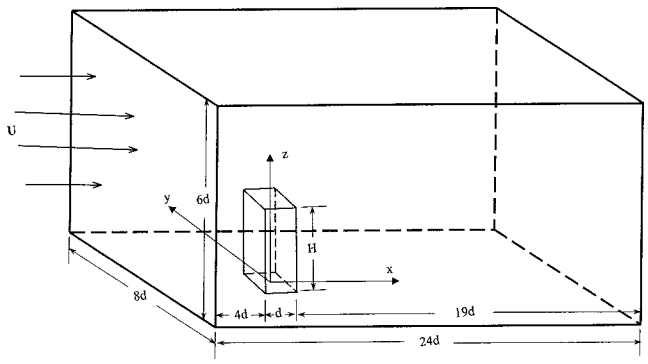

FIG. 1. Schematic diagram of the flow configuration.

shear layer vortices that the present investigation was initiated. A carefully resolved near-wall wake structure reveals here the involved process of spontaneous generation of unsteady streamwise wake vortices and their local disappearance due to vorticity cross cancellation. These streamwise vortices effectively modify the wake structure and enhance the lateral transport of longitudinal momentum from the outer stream to the wall boundary layer, which in turn accumulate a large increase in drag behind the obstacle. In view of the important roles played by the dynamics of such streamwise wake vortices in many practical applications and their presence in almost every walk of life, a detailed numerical investigation of the topic, including the evolution of the streamwise vortices through various topologically important critical points, the changing nature of their dynamics, local disappearance, and the related organized interaction mechanism, is intended to be presented here.

II. DESCRIPTION OF THE PROBLEM

Direct numerical simulations were conducted to investigate the vortex-vortex and vortex-wall interactions in the wake of a wall-mounted square cylinder (rectangular block) placed inside a channel. The square sectioned cylinder was placed symmetrically with respect to the horizontal width of the channel. We consider an orthogonal Cartesian coordinate system with origin at the center of the cylinder base (Fig. 1). The x and y axes are directed along and perpendicular to the upstream flow, respectively, coinciding with the axes of symmetry of the cylinder section at its base, whereas the z axis is directed along the axis of the cylinder. The nondimensional lengths of the channel in different directions, when normalized with respect to the width of the cylinder, are taken as follows. Since fully developed flow profiles are used at the inlet section, the upstream length $4d$ of the channel ahead of the cylinder base is assumed to be long enough to facilitate natural growth of the upstream wall boundary layer. The vertical (along the z direction) and the horizontal (along the y direction) lengths of a section of the channel with respect to the cylinder width d have dimensions $6d$ and $8d$, respectively. In order to capture the detailed three-dimensional (3D) vortex interaction process associated with the flow, the growth of fully developed boundary layers on the channel wall is essential. Moreover, the length $19d$ taken downstream of the cylinder is assumed to be long enough for the flow to

develop freely and without any influence of the downstream exit condition. In the present study simulations were performed for three different values of the Reynolds number, namely, Re=225, 300, and 500, based on the cylinder width and the incoming average channel inlet velocity. The nondimensional height of the cylinder was chosen to be $H=1.7$. A total of 14×10^5 well refined uniform control volumes were used to discretize the domain, so that every detail of the 3D shear layer interaction process involved could be captured.

III. THE GOVERNING EQUATIONS AND BOUNDARY CONDITIONS

The predictions for three-dimensional unsteady vortex interactions around a wall-mounted square sectioned cylinder were obtained by numerically solving the following nondimensional incompressible equations of continuity and momentum:

$$D\equiv\underline{\nabla}\cdot\underline{u}=0, \tag{1}$$

$$\underline{u}_t+\underline{u}\cdot\nabla\underline{u}=-\underline{\nabla}p+\frac{1}{\mathrm{Re}}\nabla^2\underline{u}. \tag{2}$$

In the equations above, all lengths have been made dimensionless with respect to the width d of the square cylinder, the velocities are normalized with respect to the average incoming velocity U at the channel inlet, and the pressure with respect to ρU^2. The Reynolds number is defined as $\mathrm{Re}=Ud/\nu$, where ν is the kinematic viscosity, ρ is the fluid density, and $\underline{\nabla}$ is the spatial gradient operator.

Boundary conditions

On the solid surfaces, the no-slip wall boundary conditions $u=v=w=0$ were used in the present study. The requirement that there can be no tangential velocity component is responsible for the generation of vortices at the wall and the development of the viscous wall boundary layer.

A zero gradient outflow condition was implemented at the downstream end of the channel, i.e., at the exit we use

$$\frac{\partial u}{\partial x}=\frac{\partial v}{\partial x}=\frac{\partial w}{\partial x}=0.$$

At the inlet section of the channel we use the following fully developed axial inlet velocity profile (White [21]) $\mathbf{u}_{\mathrm{inlet}}=[u(y,z),0,0]$ to yield a mean velocity $U=1$:

$$u(y,z)=\frac{48}{\alpha\pi^3}\beta(y,z),$$

$$\alpha=1-\frac{256}{\pi^5}\sum_{i=1,3,5,\ldots}^{\infty}\frac{\tanh(3d\xi)}{i^5},$$

$$\beta(y,z)=\sum_{i=1,3,5,\ldots}^{\infty}(-1)^{(i-1)/2}\left(1-\frac{\cosh(z\xi)}{\cosh(3d\xi)}\right)\frac{\cos(y\xi)}{i^3},$$

$$\xi(i)=\frac{\pi i}{8d}.$$

The implementation of such fully developed inlet profiles allowed us to shorten the length of the computational domain upstream of the cylinder without affecting the natural growth of the fully developed surface boundary layers. The other velocity components at the inlet are set to zero, so that any possible swirling at the inlet is ignored.

IV. NUMERICAL METHOD

A primitive variable based finite volume method was employed here to solve the set of equations (1),(2) together with the boundary conditions mentioned above, on a high-resolution uniform staggered grid system. In order to discretize Eqs. (1) and (2), the computational domain was divided into a set of staggered Cartesian cells with velocity components u, v, w defined at the arithmetic centers of the cell faces, facing toward the corresponding axial directions, while the pressure and viscosity were defined at the centers of the cells. The numerical method employed here is based on the marker-and-cell finite difference method as provided by Harlow and Welch [22], and uses second-order accurate central difference schemes in discretizations of the mass conservation equation and the pressure gradient terms. In the highly convection dominated flow addressed here, the convective terms in the momentum equations, in the interior of the computational domain, are discretized by using a third-order accurate upwind scheme, while the viscous terms are discretized by using a fourth-order accurate central difference scheme. In addition to the successful use of the scheme by a number of investigators, recent findings by Sau [15,16], Peng *et al.* [23], and Chiang *et al.* [24] revealed the reliability, stability, and accuracy of the method, which essentially prevents the occurrence of pressure oscillations in the configuration. For example, for $i\geqslant3$ ($i=1$ being the solid wall) the spatial derivatives in convective and viscous terms are approximated as below.

For $u_{i,j,k}\geqslant0$, we used

$$u\frac{\partial u}{\partial x}=u_{i,j,k}\frac{u_{i-2,j,k}-6u_{i-1,j,k}+3u_{i,j,k}+2u_{i+1,j,k}}{6\delta x}$$

and for $u_{i,j,k}<0$ we used

$$u\frac{\partial u}{\partial x}=-u_{i,j,k}\frac{u_{i+2,j,k}-6u_{i+1,j,k}+3u_{i,j,k}+2u_{i-1,j,k}}{6\delta x},$$

and the second-order derivative in the diffusion term was approximated by

$$\frac{\partial^2u}{\partial x^2}=\frac{-u_{i-2,j,k}+16u_{i-1,j,k}-30u_{i,j,k}+16u_{i+1,j,k}-u_{i+2,j,k}}{12(\delta x)^2}.$$

The above numerical scheme produced time accurate results which are quite consistent with the existing computational findings of Mason and Morton [7] and the topological sketch of the flow as provided by Hunt *et al.* [25]. A smooth

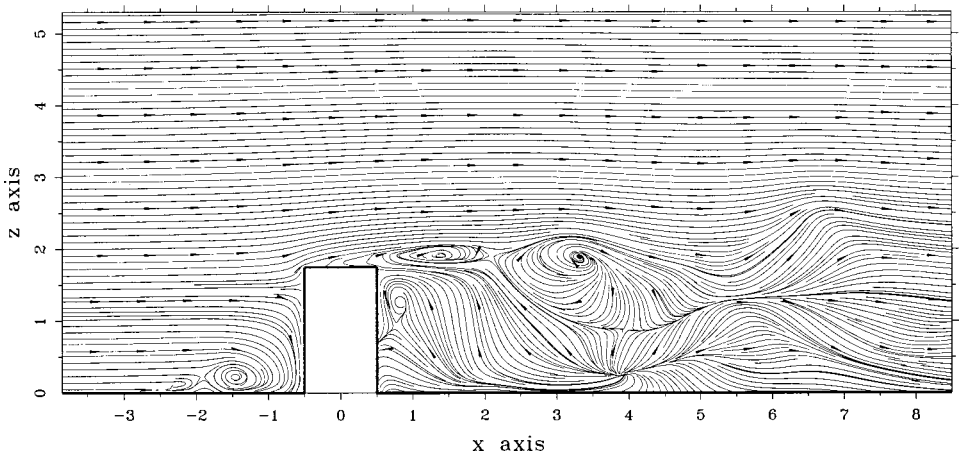

FIG. 2. Flow evolution pattern on the vertical symmetry plane ($y=0$) at $t=20$, Re=300.

flow transition was also observed at the outflow boundary. In the neighborhood of the wall boundaries, when the flow is directed away from the wall, for the discretization of the first-order derivative in the convection terms the third-order upwind method was replaced by the second-order central difference method instead of using the first-order upwind method. For example, for $i=2$ ($i=1$ being the solid wall) we used a second-order accurate central difference scheme, i.e., for $u_{i,j,k} \geqslant 0$, we used

$$u\frac{\partial u}{\partial x} = u_{i,j,k}\frac{u_{i+1,j,k}-u_{i-1,j,k}}{2\,\delta x}$$

and for $u_{i,j,k}<0$ we used

$$u\frac{\partial u}{\partial x} = -u_{i,j,k}\frac{u_{i-1,j,k}-u_{i+1,j,k}}{2\,\delta x},$$

and the second-order derivative in the diffusion term was approximated by

$$\frac{\partial^2 u}{\partial x^2} = \frac{u_{i-1,j,k}-2u_{i,j,k}+u_{i+1,j,k}}{(\delta x)^2}.$$

An explicit computational scheme was used to evaluate most of the terms in the momentum equations, while the coupling between pressure and velocities was implicit. The semi-implicit formulation was then solved with successive over-relaxation to accelerate convergence. In the recent past, the above mentioned numerical scheme has been used successfully by several investigators to solve various fluid dynamic problems. For example, among others, recently Sau [15,16], Sau *et al.* [18], Peng *et al.* [23], Chiang *et al.* [24], and Wissink [26] have successfully implemented the solution algorithm and the numerical scheme to study the onset of unsteady 3D flow development through different complex geometries. To be sure about the correct choice of the computational scheme, we ran a series of test cases with different fourth-order and seventh-order (Wissink [26]) accurate upwind schemes; however, the present method was observed to be efficient enough in accurately predicting the associated flow phenomena that are reported in the literature.

In the computation, velocity components were first advanced explicitly using the previous state of the flow, having calculated the accelerations caused by convection, diffusion, and pressure gradients through a time step δt. The solution was then advanced in time using a semi-implicit scheme that is formally second-order accurate. While advancing t, the time step δt was so chosen that it always satisfied the Courant-Friedricks-Lewey (CFL) stability criteria. Then the adjustment of pressure and velocity was done by an iterative process in order to ensure mass conservation in each cell. This iterative correction of the velocity field through the implicit continuity equation is equivalent to the solution of the Poisson equation of pressure. The iterative process was repeated until the sum of D values for all cells became less than 10^{-4}. Computations were carried out on a parallelized system of Pentium 1900 MHz processors, in a domain with a spatial resolution of $244\times101\times71$ grid points. In addition to the main production runs for which results are presented here, several short simulations were conducted to examine the necessity of using different higher order discretization

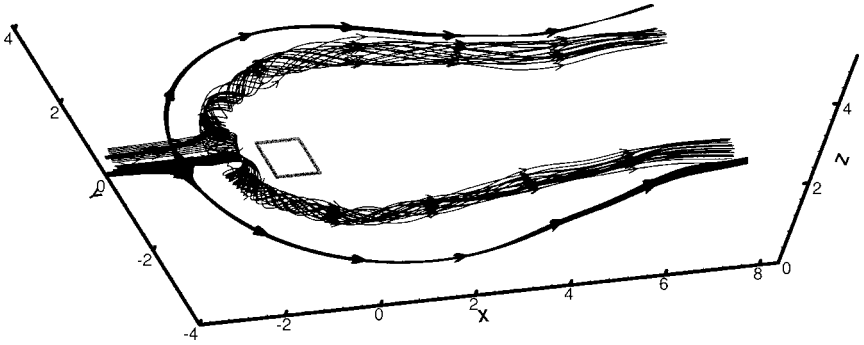

FIG. 3. Instantaneous streamlines showing the horseshoe vortex formation at $t=20$, Re=300.

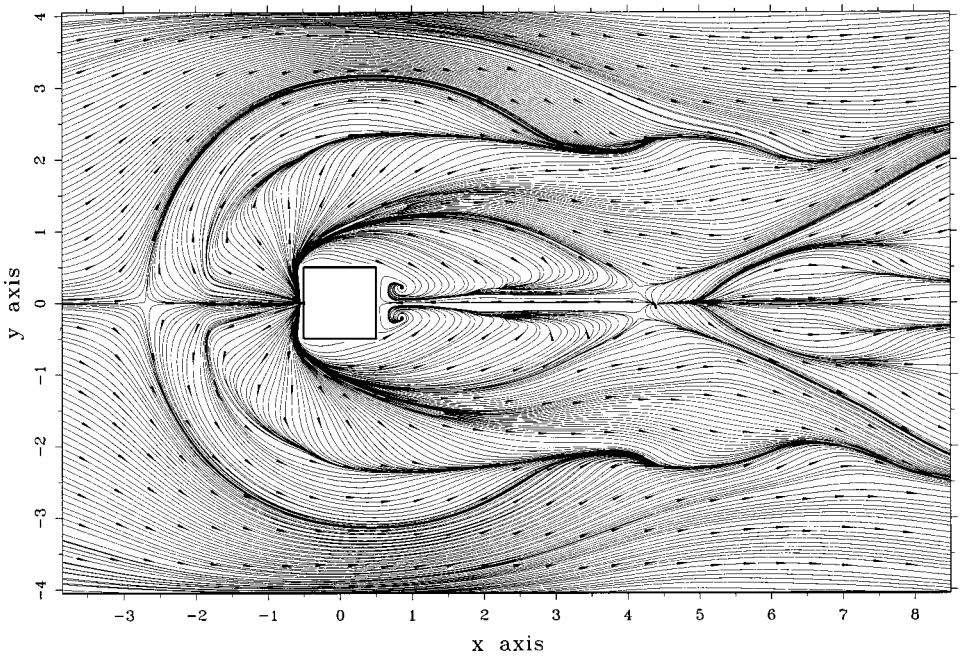

FIG. 4. Near-wall streamline pattern indicating the arrangement of critical points on the channel floor at $t=20.0$, Re$=300$.

schemes for the convective terms in order to be sure about the accuracy of the presented results. It may be noted that each simulation performed here took about 2000 h of CPU time in the above mentioned computer system. Furthermore, a grid sensitivity study was performed at various stages of the computation to verify the quantitative accuracy of the results presented, and the optimum grid resolution was used. To preserve the essence of the realistic nature of the flow, we performed very extensive and careful flow simulations in the full domain of the physical problem.

V. RESULTS AND DISCUSSION

In a recent work, Sau *et al.* [18] investigated various sources of vortices observed in the near field of a square jet in a cross flow, and it was verified that the vortices originate either from the cross-flow channel floor or from the jet shear layer. The vortices that originate from the channel floor shear layer (see also Fric and Roshko [19]) subsequently spiral and lift themselves away from the cross-flow wall to join the main stream. Such vortices are often termed upright vortices. The present investigation exploring vortex interaction around a wall-mounted square cylinder was initiated with the view of examining the fundamental differences in the generation mechanisms of the vortices in the two systems and their downstream interaction processes. The downstream vortex-vortex and vortex-surface interaction patterns in the present flow configuration and the associated process of diffusive annihilation of vortices by vortices of the opposite sense, as generated from the flat wall boundary layer, however, appeared to be interesting. The primary effect of such an obstacle is to create disturbance pressure around the cylinder, which slows down fluid directly approaching the body, and accelerates it laterally either over or around the body. Here it has been shown that the generated vortices issuing upstream or from the cylinder surface are subsequently entrained into

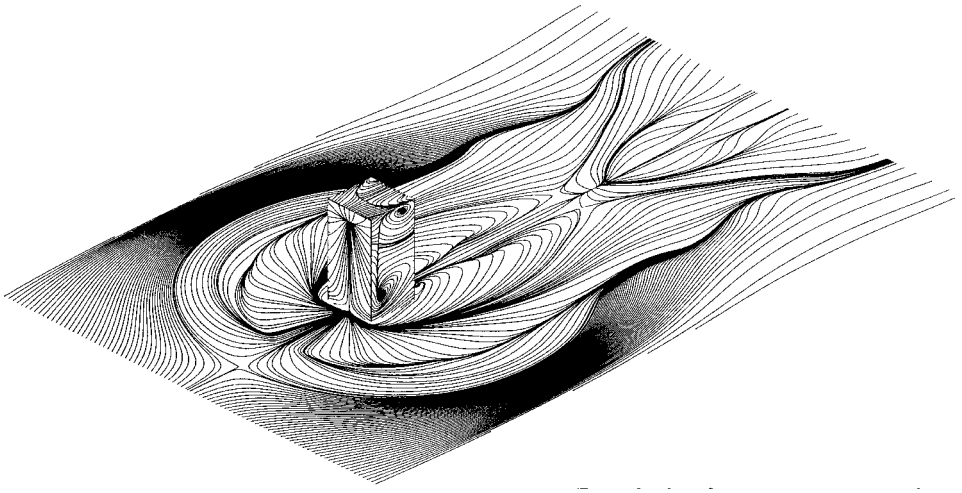

FIG. 5. Surface flow topology on the cylinder and on the channel floor at $t=14$, Re$=300$.

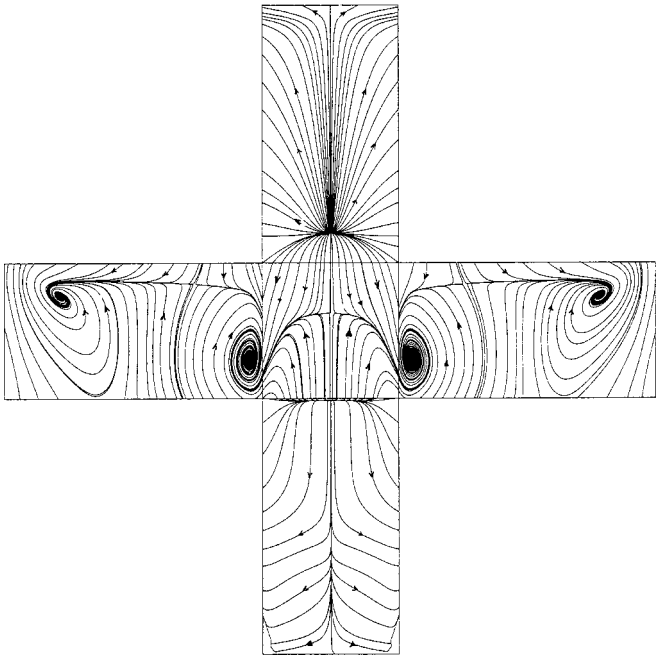

FIG. 6. Complete view of surface flow topology over the cylinder at $t=14$, Re$=300$.

the downstream flow along with the boundary layer vorticity and are subject to inertial turning and stretching.

A. Horseshoe vortex formation and topology of flow separation

Figure 2 demonstrates the representative symmetry plane flow behavior and indicates the formation of the upstream horseshoe vortex around the cylinder-plate junction at $t=20$. The Reynolds number of the approaching flow with respect to the average velocity at the channel inlet and the cylinder width is 300. The instantaneous streamlines as depicted in Fig. 3 reveal the two-loop structure of the horseshoe vortex, with their tails extending over the downstream floor boundary layer. Here we may mention that in the case of a jet in a cross flow with the base section of the cylinder being used as the flush-mounted jet orifice, the jet momentum together with upstream and the vertically upward flow evolution from a symmetry plane node situated immediately behind the jet essentially helped to entrain the tails of the horseshoe vortex (Sau *et al.* [18], Kelso *et al.* [20], and Yuan *et al.* [27]) upward along the lee side of the jet. The counter-rotating vortex pair (Sau *et al.* [18] and Kelso *et al.* [20]) which remains active in the downstream jet region provides further lift in entraining the horseshoe vortex tails. Figure 4 displays the near-wall topological flow evolution pattern around the cylinder through various critical points, facilitating the growth of the horseshoe vortices. Notably, besides the presence of the upstream saddle (Fig. 4) on the channel floor and the node (Fig. 2) on the vertical symmetry plane $y=0$, the flow topology in Fig. 4 reveals the formation of two spiraling foci immediately behind the cylinder base, and the formation of two symmetrically placed downstream saddles near $x=4$. It may further be noted from Fig. 4 that

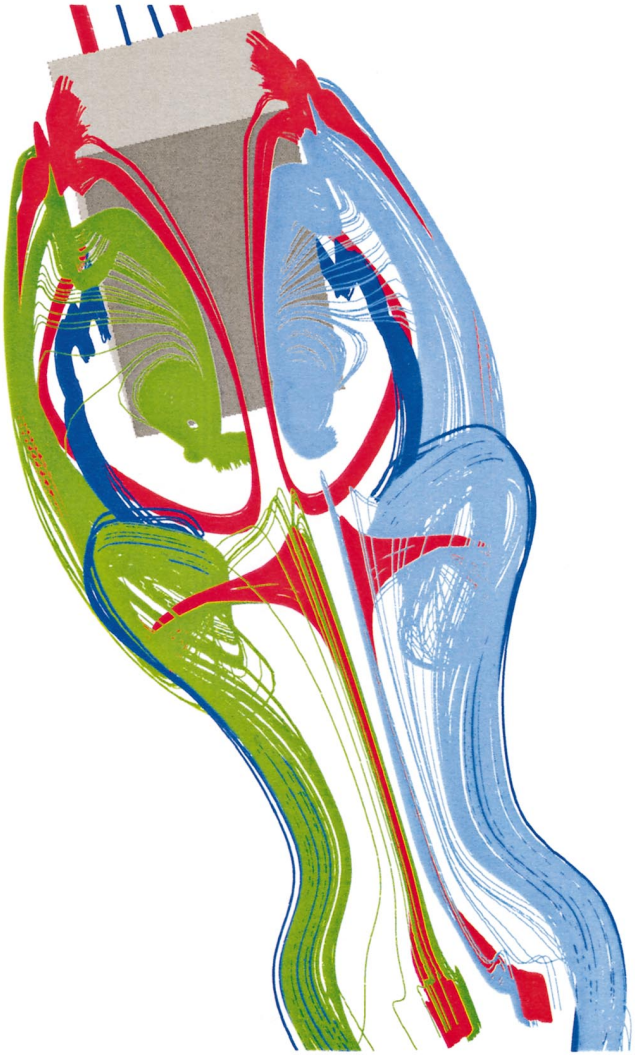

FIG. 7. (Color) Evolution of fluid particles issuing from topological singular points at $t=14$, Re$=300$.

there appears local contraction of the downstream wake and convergence of the upstream limiting streamlines around $x=4$. This local contraction of the wake, as will be shown later, remains implicitly associated with significant vorticity cancellation in the region and therefore suggests possible wake disappearance. Notably, at Re$=300$, the observed slight temporal variation of the location of the horseshoe vortex centers on the vertical plane of symmetry (Fig. 2) and the small spatial shifting with time of the topological critical points (e.g., Fig. 4) situated near the cylinder base suggest that near the upstream part of the body the vortices maintained a quasisteady state during their temporal evolution. In fact, during time evolution the entire topological arrangement of the critical points (e.g., Figs. 4–6) as a whole remained invariant. However, while approaching the downstream side of the obstacle the vortices exhibit predominantly unsteady characteristics (e.g., Fig. 9 below). On the other hand, as will be shown later, with the increase in Reynolds number, not only did the locations of the horseshoe vortex centers on the symmetry plane ($y=0$) move away (upstream) from the obstacle, but the existence of the

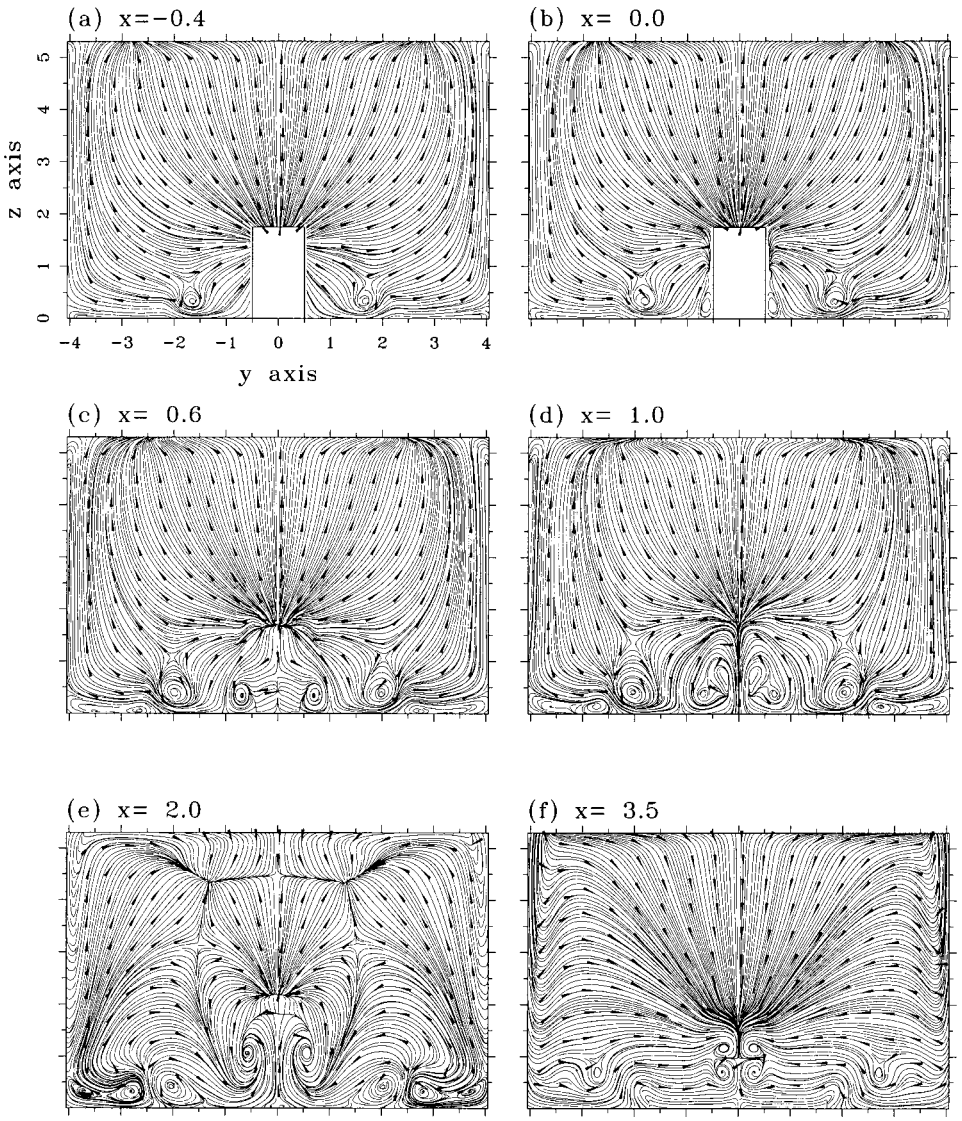

FIG. 8. Streamline pattern on different vertical transverse (x) planes for Re=300 at $t=20$.

second horseshoe vortex became more clear and there appeared significant distortion of the downstream floor topology. Notably, on the plane of symmetry, the streamlines (Fig. 2) indicate that the lee separation for the flow is characterized by a spiral mode with downwash remote from the body (see also Mason and Morton [7]). Moreover, the separation structure on the downstream surface of the cylinder consists of an attachment line (for instance, see the topological flow evolution pattern in Fig. 6), with attached streamlines originating from a downstream spiral node, which is a source. Streamlines through the top of the cylinder end in a spiral mode, and the shedded rear separation bubble gradually moves downstream with time. During the entire course of flow evolution, the presence of the downstream spiral node was always experienced slightly above the flat boundary (as indicated by Fig. 2) and it exhibited slight unsteady back-and-forth streamwise motion. A similar downstream symmetry plane node formation was observed to take place (e.g., Sau *et al.* [18] and Kelso *et al.* [20]) even behind a jet in a cross flow. The height of the node from the flat wall and its distance from the downstream edge of the obstacle, however, continued to vary slowly with time. Such unsteady effects will later be shown to intensify gradually with an increase in Reynolds number. It is important to note that the computed symmetry plane flow topology (Fig. 2) remained very much consistent with the previous predictions as made by Hunt *et al.* [25]. Another important observation worth mentioning here is that the presence of the downstream node on $y=0$ obstructs the formation of a closed symmetry plane separation bubble in the wake of a wall-mounted obstacle. Notably, such findings remain quite consistent with the observations reported by Hunt *et al.* [25] and by Counihan *et al.* [28].

In order to better represent the complete three-dimensional flow development process through all the existing critical points on and around the cylinder, a combined view of the topological flow evolution (at Re=300 and $t=14$) over the channel floor and the cylinder surface has been explicitly provided in Figs. 5 and 6. The floor boundary layer while approaching the cylinder is seen to separate in the form of two distinct horseshoe vortices. The oncoming fluid moves both downward and upward from a node (Fig. 5) on the upstream cylinder surface and separates from the top and the lateral (cylinder) surfaces. The streamline pattern on the vertical symmetry plane (Fig. 2) clearly supports such a

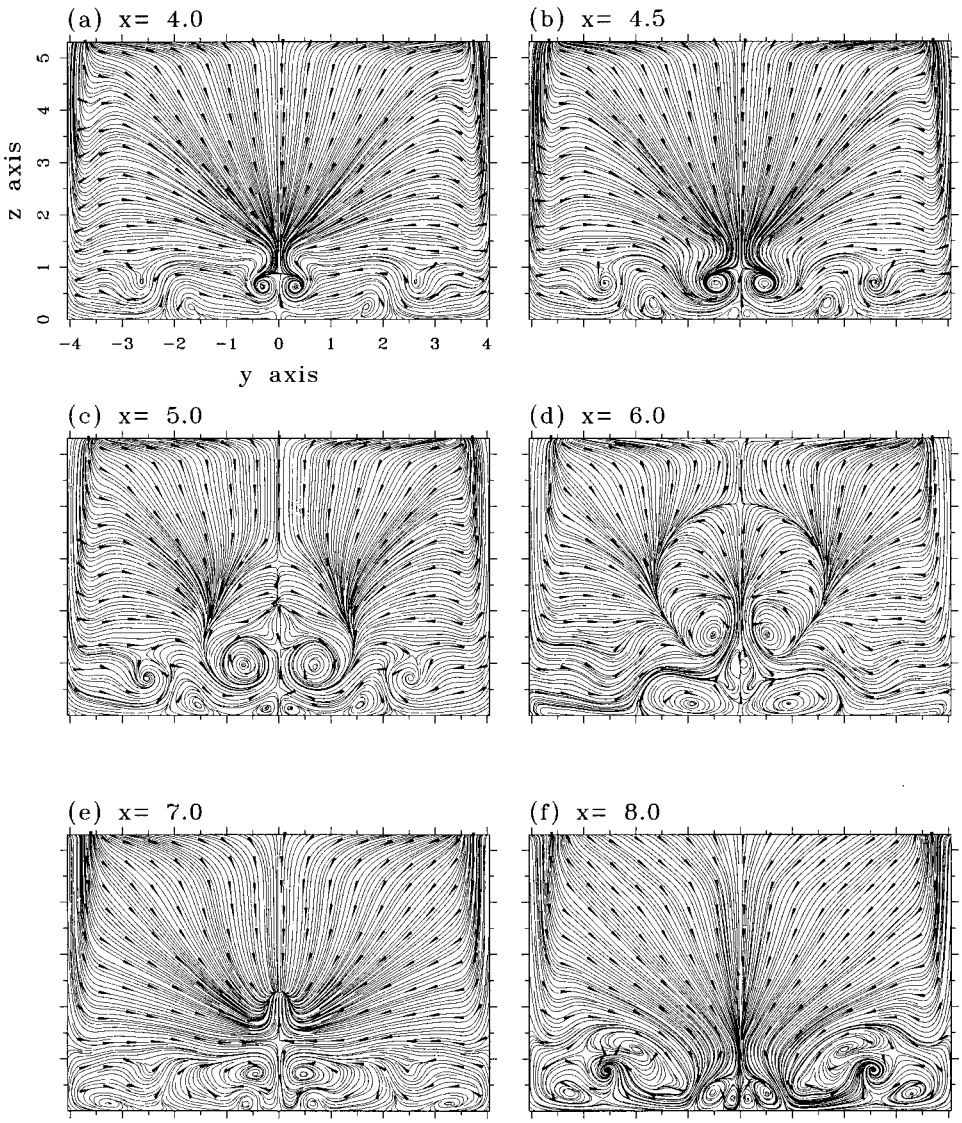

FIG. 9. Flow evolution pattern through different vertical transverse (x) planes for Re=300 at $t=20.0$.

fluid motion on the upstream and the downstream surfaces of the cylinder. The separated flow from the top moves downstream, but the presence of a node (Fig. 2) on the vertical symmetry plane does not allow any downstream flow reattachment to the channel floor. Notably, the flow topology on the front surface (as viewed from Fig. 1) of the cylinder reveals the formation (Fig. 5) of a pair of spiraling nodes and a saddle between the nodes. The major flow separation from the front surface takes place in the form of spiraling vortical flows around two clearly defined vortical corelines issuing out of these two spiraling nodes, one of which is situated close to the bottom of the cylinder, while the other one forms near the front top corner. Vortices originating from the spiraling nodes on the front (lateral) cylinder surface are expected to extend far downstream and contribute streamwise vortices to the developing wake. The flow developed at this Reynolds number, however, appears symmetric with respect to the vertical central plane ($y=0$) passing through the cylinder axis, and a similar flow separation process with the same topological signature is also observed through the rear surface of the cylinder. A complete picture of the topological flow evolution pattern over the cylinder surfaces is presented in Fig. 6. The left and right wings of the picture reveal the flow topology on the two lateral (front and the rear) sides of the cylinder, which are indeed symmetric. The top and bottom parts represent the flow topology on the upstream and downstream surfaces of the cylinder, while the central square section represents topological flow evolution over the top surface of the cylinder. Notably, with increased Reynolds number the separation line on the top of the cylinder continues to move upstream, toward the top leading edge. In addition, a combined view of the representative symmetry plane flow behavior (e.g., Fig. 2) and the flow topology on the downstream surface of the cylinder (Fig. 6) reveals that the upstream moving fluid (Fig. 2) originating from the spiral node (which is a source) that formed slightly behind the cylinder reattaches to the downstream surface of the cylinder, and the reattaching fluid does not originate from upstream. Such findings remain quite consistent with the previous predictions made by Mason and Morton [7]. Moreover, here it is important to note that the computed *surface flow topology*, as revealed by Figs. 5 and 6, appears to satisfy the following topological constraint [involving nodes (N), half nodes (N'), saddles (S), and half saddles (S')] of Hunt *et al.* [25]:

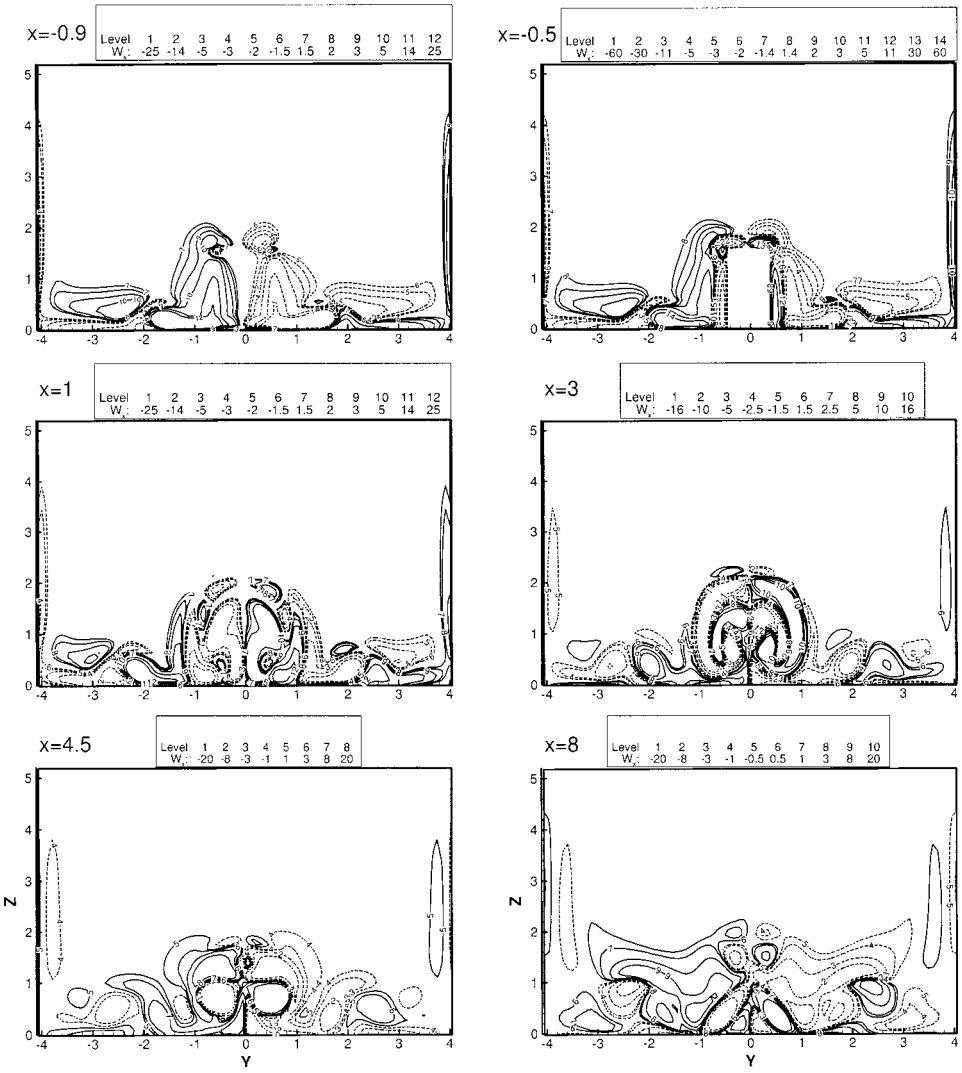

FIG. 10. Contours of streamwise (ω_x) vorticity on different x planes for Re=300 at $t=20$.

$$\left(\sum N+\frac{1}{2}\sum N'\right)-\left(\sum S+\frac{1}{2}\sum S'\right)=1-n$$

with $n=1$, in the presence of seven nodes, one half node, six saddles, and three half saddles (in the surface flow topology).

Figure 7 demonstrates the important three-dimensional evolution details of the fluid particles (streamlines) issuing directly from four topological nodes that form on the two lateral surface shear layers of the cylinder (Figs. 5 and 6) and the two recirculating foci (Fig. 4) which develop on the floor boundary layer immediately behind the base of the cylinder. The blue and the red colored streamlines, upon issuing from two pairs of symmetrically placed bottom and top nodes on the two lateral surfaces of the cylinder, are seen (Fig. 7) to move downstream while spiraling around their vortical corelines. On the other hand, the green and the cyan (sky-blue) colored streamlines (Fig. 7) constitute a pair of upright vortices, which originate from the two tornadolike critical points (spiraling foci) that develop on the channel floor shear layer immediately behind the cylinder base (Fig. 4). The vortices subsequently leave the channel floor vertically and move downstream while spiraling around their corelines. The important issues that may be noted here is that the streamlines (Fig. 7) issuing from these symmetrically placed nodes constitute vortices of opposite strength, and due to the developed strong transverse pressure gradient these vortices (of opposite strength) come closer at a downstream location, leading to significant local contraction of the wake (Fig. 7). As these opposite strength vortices of different generic origin interact with each other, there appear significant vorticity cancellation at some downstream location, leading to considerable shrinking and disappearance of the near-wall wake. At this point we would like to mention that the streamlines issuing from the topological critical points, as presented in Fig. 7, appear as an envelope around the downstream wake. All other separated fluid particles issuing from the sharp edges of the cylinder are observed to fall, more or less, within the three-dimensional wake structure presented in Fig. 7. Extensive details about the process of wake development and its local disappearance due to vorticity cross cancellation (i.e., due to close interaction among vortices of opposite strength, originating from the two different sides of the cylinder) are presented in the next section.

It may be noted that while the presently simulated overall flow structure remained very much consistent with the findings of Mason and Morton [7], the downstream vortex shed-

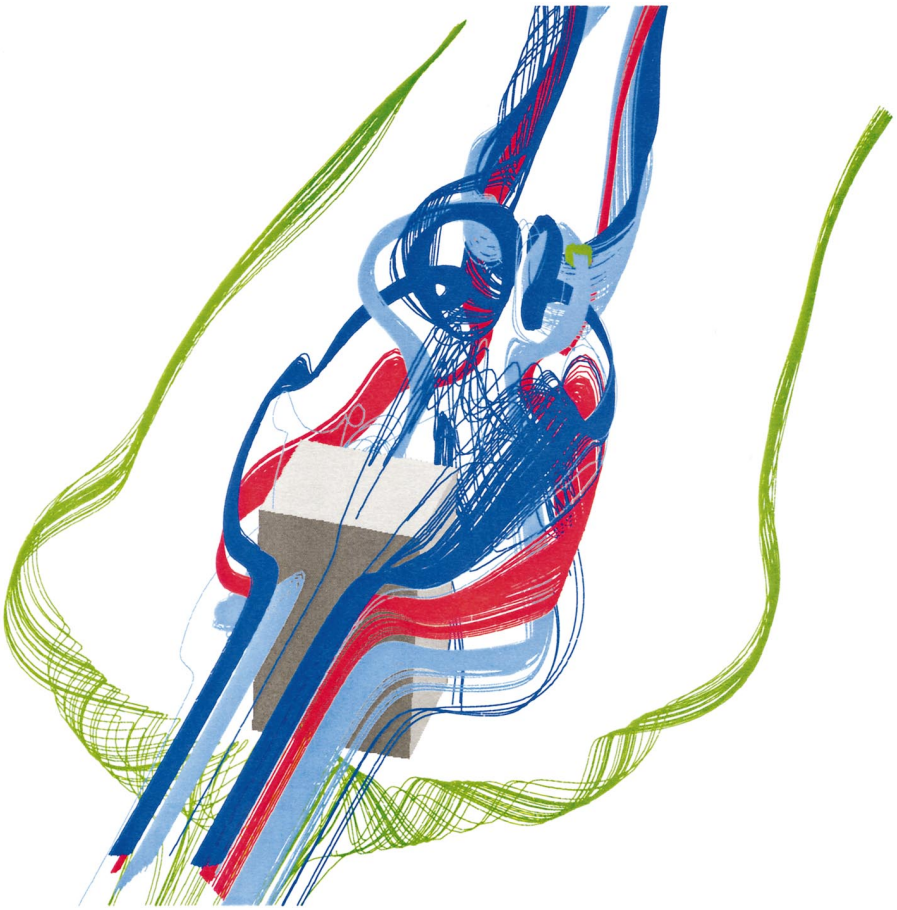

FIG. 11. (Color) Three-dimensional view of the flow evolution pattern revealing the downstream vorticity cancellation and local disappearance of the wake at $t=20$, Re$=300$.

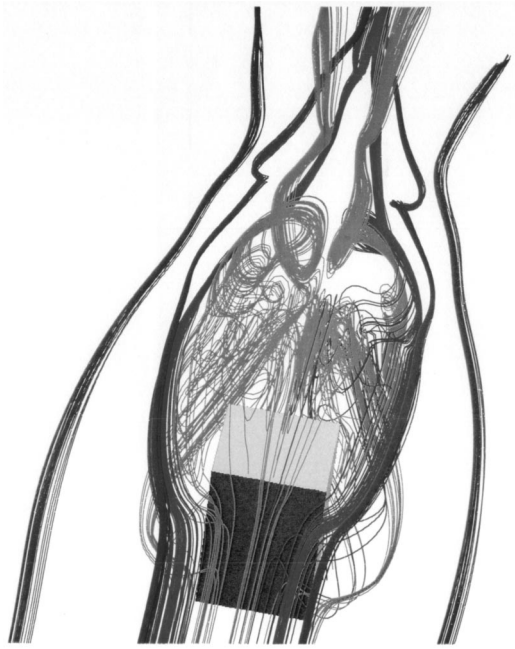

FIG. 12. Three-dimensional flow evolution pattern revealing the process of downstream vorticity cancellation and local disappearance of the wake at $t=20$, Re$=300$.

ding was not observed by them. This is because of the lower values of Reynolds number used by Mason and Morton [7], as they opted to establish a guideline for the steady flows. Another important feature of these flows worth mentioning here is that, in our recent study of a square jet in a cross flow, the vortices were observed to originate either from the jet shear layer or from the cross-flow boundary layer. Such sources of vorticity production around a round jet have also been experimentally confirmed by Fric and Roshko [19]. Interestingly, vortices around a wall-mounted obstacle are observed to evolve from the surface shear layers. In addition, the topological flow evolution pattern from the flat wall (e.g., Fig. 4) just downstream of the cylinder facilitates the formation of two spiraling nodes (foci). These are the places from where the accumulated boundary layer vortices spiral in and subsequently lift themselves away from the bottom channel surface (Fig. 7) in the form of tornadolike upright vortices to finally join the far-wall downstream wake. Note that the development of such upright vortices from the spiraling critical points (foci) on the channel floor has been both experimentally (e.g., Fric and Roshko [19] and Kelso *et al.* [20]) and computationally (Sau *et al.* [18]) confirmed behind a jet in a cross flow. The striking difference for the flow over a wall-mounted cylinder is that here we observed the formation of only one pair of such upright vortices, whereas the topological separation pattern behind a jet allowed the growth of at least two such pairs of (upright) vortices (Sau *et al.* [18] and Fric and Roshko [19]). Of course, no vortex shedding appears behind a jet in a cross flow.

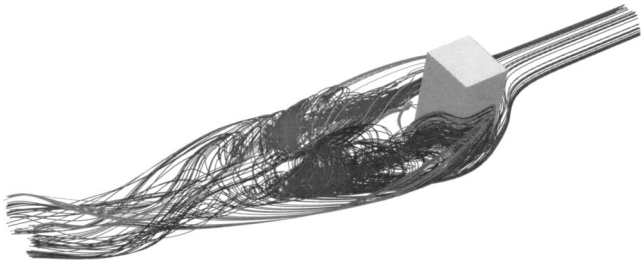

FIG. 13. Three-dimensional view of the flow evolution pattern revealing the downstream vorticity cancellation and the local disappearance of the wake at $t=20$, Re$=225$.

B. Disappearance of wake

In order to better understand the flow physics and demonstrate the analogy of the present findings with the existing literature (e.g., Mason and Morton [7]), at this point it is important that here we present the detailed vorticity dynamics and the vortex-wall interaction process around the cylinder. Figures 8 and 9 present the transverse sectional view of the wake and the near-wall interaction of the vortical structures through different streamwise stations at $t=20$ and for Re$=300$. The streamline pattern along the front half of the cylinder reveals that the flow is mostly accelerated upward and outward as it is diverted around the obstacle. The shear layers on the bottom half of the cylinder are seen to get deflected laterally downward (Fig. 8) at $x=-0.4$ and spread over the flat bottom wall. The uniform vertical flow along the upstream cylinder surface is presumably the result of excess thickening of the Blasius boundary layer. As we move on to the central section ($x=0$) of the obstacle, the shear layer thickening is seen to become more prominent. It is important to note that on the transverse vertical plane ($x=0$) through the axis of the cylinder, the folding of the lateral shear layer has led to the inception of a pair of streamwise vortices near the flat wall $z=0$. Notably, these vortices are neither the downstream tails of the horseshoe vortex, nor the streamwise extensions of any other upstream vortex. On the other hand, the second pair of symmetrically placed vortices, which are observed to form away from the cylinder surfaces and placed slightly above the bottom plane, is actually the downstream extensions of the horseshoe vortex tails. Moreover, sectional streamline patterns through different transverse planes (Figs. 8 and 9) suggest the spontaneous generation of the streamwise vortices and the shear layer rollers behind the cylinder, which remained extended far downstream. Here it is important to mention that the generation mechanism of the central pair of vortices, which are observed to originate near the minor (y) axis ends of the cylinder base section on $z=0$ from the laterally folded shear layer, is in a sense similar to the vortices that evolved as the counter-rotating vortex pairs for the bent-over jet in a cross flow (e.g., Kelso *et al.* [20] and Yuan *et al.* [27]).

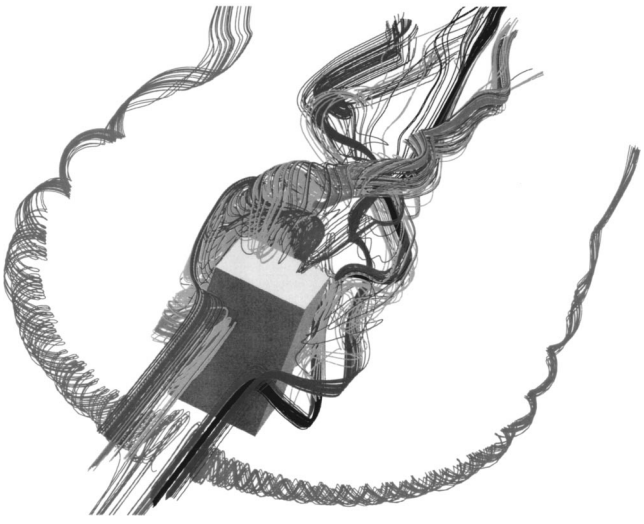

FIG. 14. Three-dimensional flow evolution pattern revealing the process of vorticity cancellation and local disappearance of the wake at $t=14$, Re$=500$.

Figure 8 also displays the gradual intensification in the generation of near-wall wake vortices and the process of mutual vortex-vortex and vortex-surface interactions within $0.0\leqslant x\leqslant 2.0$. Remarkably, in the range $3\leqslant x\leqslant 4$ a significant disappearance of the near-wall wake interaction is observed, and at $x=4$ we encounter the existence of only one mushroomlike floating vortical structure (Fig. 9), near the central channel section, which has already left the flat wall. Two other pairs of distant eddies, however, exist on $x=4$, but they are essentially the extended tails of the two upstream horseshoe vortices. Notably, soon after the near-wall wake locally disappeared, the far-field flow evolution pattern was seen to change from its upstream monopolar to its downstream dipolar form. Such a flow evolution process (as will be shown later) became more prominent at a higher Reynolds number, and remains consistent with the predictions made by Hunt and Eames [10]. Notably, for $x\geqslant 5$ we observe that the near-wall vortical wake development gradually gains momentum again, and it is enhanced with downstream distance. However, it may be carefully noted that the nature of circulation of the near-wall central eddies (which are symmetrically placed around the vertical central line) appears to be opposite for $0\leqslant x\leqslant 2$ and $6\leqslant x\leqslant 8$. Notably, the near-wall flow topology as depicted in Fig. 4 indicates the formation of a pair of symmetrically placed saddles near $x=4$ and a node on the vertical plane of symmetry ($y=0$), which may be better viewed in Fig. 2. Furthermore, the significant near-wall wake disappearance in the region $3\leqslant x\leqslant 4$ (Figs. 8 and 9) is seen to remain closely associated with convergence of the limiting streamlines and the local contraction of the wake (Fig. 4) near $x=4$. Such structural evolution of the near-wall wake was encountered during the entire course of time evolution. The local flow acceleration in opposite directions around the line of symmetry ($y=0,z=0$) (Fig. 4), in the presence of the node on the vertical symmetry plane (Fig. 2), presumably induces vorticity cancellation within $3\leqslant x\leqslant 4$ and helps to generate streamwise vortices of opposite sense in the upstream and downstream (Fig. 10) regions. The near-wall fluid particles behind the cylinder are seen (Figs. 4 and 5) to turn around and move upstream (along the line of symmetry) through the saddles, and eventually form a pair of spiraling foci near the downstream edge of the cylinder. The fluid

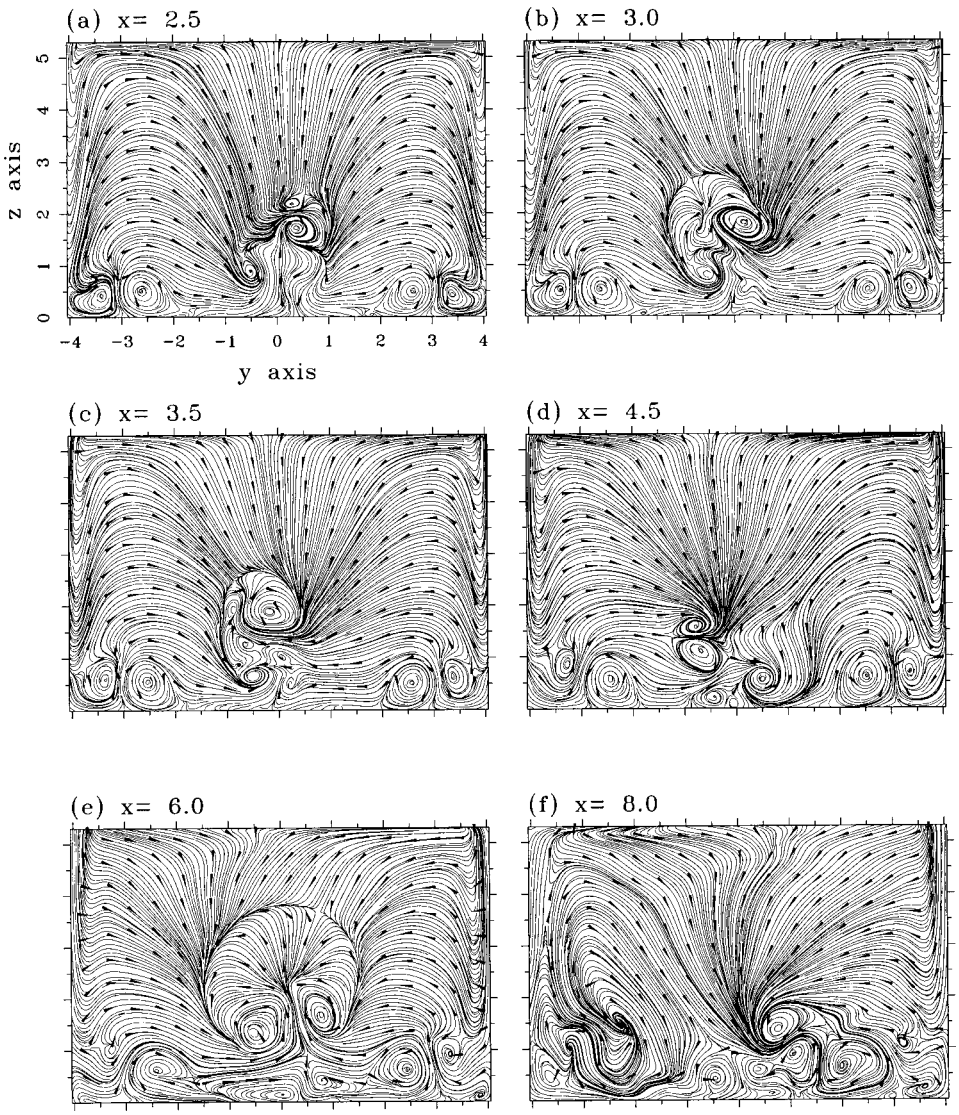

FIG. 15. Unsteady eruption of shear layer structures at different streamwise stations for Re=500 and $t=14.0$.-

particles that fall outside this loop experience smooth downstream passage beyond the saddles. Importantly, these findings remain consistent with the predictions recently made by Hunt and Eames [10] and the critical nature of the associated flow as sketched by them in their Fig. 1. We guess the sudden change in flow pattern around the saddles (which are also points of local pressure maxima) may be responsible for the local disappearance of the wake in the region. Since the developed far-wake flow behavior maintained its predominantly unsteady characteristics, here it is important to mention that a very similar process (as observed in Figs. 8 and 9) of eruption of the near-wall wake vortices and their disappearance within $3 \leqslant x \leqslant 4$ was observed to take place at every instant of time, but the lack of space restricts us from presenting those in further detail. Furthermore, as will be shown later (e.g., Fig. 15) a similar process of local near-wall wake annihilation through vorticity cross cancellation is experienced at a higher Reynolds number Re=500 also.

In order to gain better insight into the phenomenon of wake disappearance it is important that here we explore the three-dimensional details of the physical flow evolution process. It may be noted once again from Fig. 9 that at Re $=300$ and $t=20$, significant reduction of the near-wall wake vortices appears in the range $3 \leqslant x \leqslant 4$, where streamlines spiral into relatively few symmetrically placed far-wall vortical structures. Our interest is to investigate both upstream and downstream evolutional details of the streamlines which pass through these symmetrically placed far-wall vortical cores. In Fig. 11 we have depicted streamlines passing through all the vortical cores that remained present on $x=3.5$ (Fig. 8), and different colors are assigned to the streamlines to demonstrate the fact that they pass through a pair of such symmetrically formed vortical cores. Notably, the streamlines (of a particular color) passing through one side of the cylinder possess vorticity of opposite nature with respect to those passing through the other side of the cylinder. It is important to note (Fig. 11) that in the near wake of the cylinder a very complex and chaotic interaction of these streamlines takes place, suggesting close three-dimensional interaction of various supporting vortices of opposite strength. After a series of such complex interactions, leading to mutual annihilation of the supporting vortices, the streamlines with different origins are seen to merge together (or at

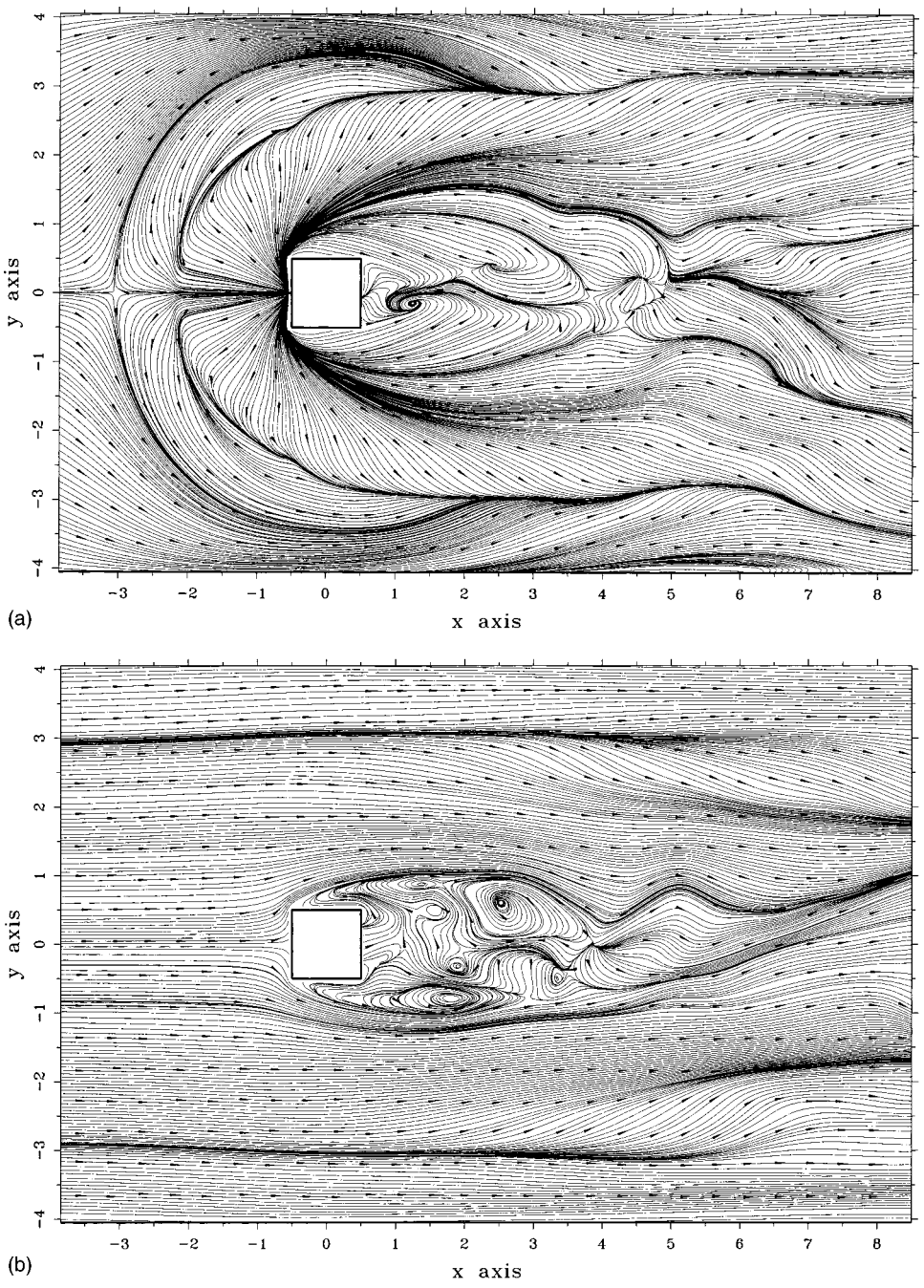

FIG. 16. (a) Arrangement of near-wall critical points on $z=0.01$ around the cylinder at $t=14$ and Re$=500$. (b) Sectional view of the wake structure on $z=1$ for Re$=500$ and $t=14$.

least get fairly close) at the far end of Fig. 11. Such findings are consistent with the streamline behavior we encountered at $x=4$ in Fig. 9. The recirculating vortices that formed at the bottom corner regions (Figs. 8 and 9) are in fact the extended tails of the two horseshoe vortices (Figs. 3 and 11). Furthermore, it is important to note that the extended tails of the horseshoe vortices did not join the vorticity interaction process, and even at a far downstream location they retained their noninterfering identity with respect to the core vortices. Here we may recall that Mason and Morton [7] in their study also postulated that the horseshoe vortices do not get involved in the vorticity interaction process. In order to further reveal the wake development process beyond $x=4.5$, in Fig. 12 we depict the evolutional details of the streamlines passing through the vortical cores on $x=4.5$ that may be viewed from Fig. 9. Notably, as in Fig. 11, the streamlines in Fig. 12 display their very chaotic mutual interaction in the near wake (within about three cylinder diameters downstream). Then, between the far wake and the near wake significant cancellation of the vortices and contraction of the wake appears before they spread again. Notably, a combined view of the sectional wake behavior for $3 \leqslant x \leqslant 4$ (Figs. 8 and 9) and the channel floor flow topology (Fig. 4), together with the depicted vorticity annihilation as presented in Fig. 12, suggest that during the course of flow evolution the phenomenon of wake disappearance remains intrinsically associated with its local contraction (see also Fig. 7). The dominance of the transverse pressure gradient between the near wake and the

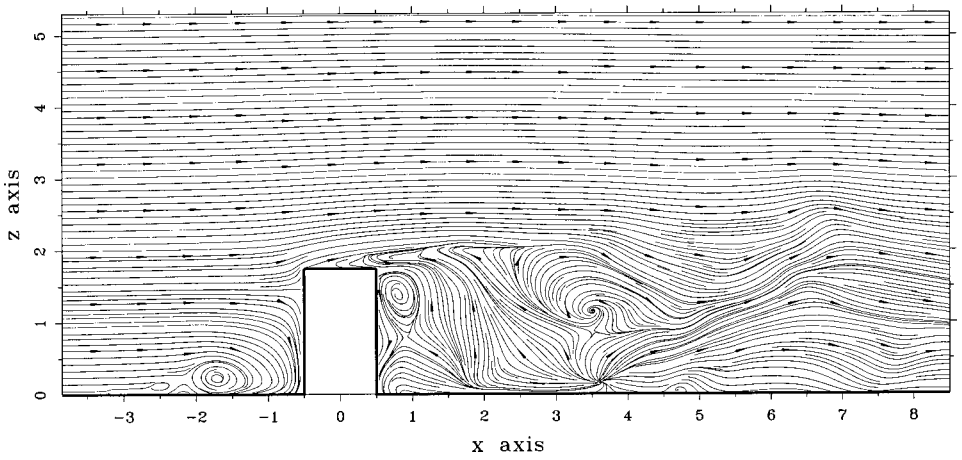

FIG. 17. Vortical flow evolution pattern through the vertical plane of symmetry ($y=0$) for Re $=500$ and $t=14$.

far wake, which essentially is maximum across the downstream saddles (Fig. 4), is believed to force such a contraction of the wake. At this point readers may refer to the recent work of Hunt and Eames [10], where the authors also predicted that the phenomenon of wake disappearance should remain closely connected with the local contraction of the streamlines. In Fig. 13 we demonstrate the process of streamwise wake annihilation at $t=20$ and Re$=225$. Here the depicted streamlines (Fig. 13) pass through the four different symmetrically placed vortical cores that developed on the plane $x=3.5$. It may be clearly noted that the streamlines originating from one side of the cylinder possess vorticity of opposite nature with respect to those issuing from the other side. Interestingly, as in the previous cases, here also the wake vortices are observed to get diffused significantly at some downstream location, due to mutual interaction of the governing streamlines (possessing vorticity of opposite sign). However, the relatively lower value of the Reynolds number (Re$=225$) used in this case apparently delays the corresponding wake annihilation. To further demonstrate the physical process of vorticity cancellation and the flow mechanism leading to local wake disappearance, in Fig. 14 we depict the streamlines, for Re$=500$ and $t=14$, which pass through the vortical cores over $x=2.5$ (Fig. 15). Notably, in this case also the observed complex interaction process of these streamlines (possessing vorticity of opposite strength) leads to the significant cancellation (Fig. 14) of the near wake behind the cylinder. Moreover, at about two cylinder diameters downstream a remarkable contraction of the near wake appears, where vortices of different origins merge together upon losing their strength. Thereafter, the wake is seen to spread again along the channel floor. Here it is important to note that the sectional view of the wake as presented in Fig. 15 also reveal the notable reduction in the near-wall wake within $2.5 \leqslant x \leqslant 3$ and its continued spreading beyond $x=4.5$. Furthermore, the corresponding flow topology depicted in Fig. 16(a) also demonstrates the locally contracting behavior of the wake within $2.5 \leqslant x \leqslant 3.5$. At this point we may mention that, despite the fact that the issue investigated is quite complex and difficult to demonstrate physically, the findings from the present simulation remain very much consistent with the recent predictions on the topic as made by Hunt and Eames [10].

C. Influence of Reynolds number

Figure 17 reveals the flow evolution details on the vertical symmetry plane ($y=0$) for Re$=500$. First, it may be noted that the center of the horseshoe vortex at this increased Reynolds number has moved significantly upstream. Second, the entire downstream wake on the symmetry plane (Fig. 17) is seen to become compressed and move closer to the cylinder, including the near-wall downstream node (which is now seen to form near $x=3.6$). As a result, the downstream part of the cylinder in this case experiences far more impact from the unsteady wake vortices. Moreover, at Re$=500$, the observed [Fig. 16(a)] distortion in the downstream channel floor flow topology (which continues to vary continuously with time) suggests the possible occurrence of symmetry breaking flow bifurcation behind the cylinder and demonstrates the key near-wall features of the flow, which contributes to the development of truly asymmetric and unsteady far-wall flow [Fig. 16(b)]. As far as eruption of the downstream floor shear layer is concerned, Fig. 15 indicates that the process has already been initiated with the random generation of the mushroomlike vortical structures from the downstream boundary layer. The erupted floor shear layer at this increased Reynolds number evolves in a rapidly growing asymmetric (Fig. 15) manner, partly due to local dominance of the strong transverse flow and because of enhanced unsteady vortex-surface interaction in the region. Notably, the observed random growth (Fig. 15) of these mushroomlike structures from the downstream floor shear layer is reminiscent of recent experimental findings of Seal and Smith [6] (as presented in their Fig. 7) and Wallace and Balint [29], revealing the eruption and bursting phenomena involved. Further investigation of the detailed flow transition process is in progress and intended to be addressed in another work.

D. Concluding remarks

In the present study, three-dimensional flow evolution through a surface-mounted square cylinder has been simulated numerically. While near the upstream part the floor boundary layer vortices are observed to get deflected laterally upon encountering the cylinder and separate in the form of a pair of horseshoe vortices, their downstream extended tails are found to contribute vortices in the far wake. The

developed flow is also seen to separate from the top and the lateral surfaces of the cylinder through several topologically important critical points. The vortices originating from the lower part of the lateral cylinder surfaces are seen to leave the surface and extend far downstream, and contribute streamwise vorticity in the near-wall wake. Because of the sharp pressure difference generated along the cylinder edges, the approaching flow generates additional streamwise vortices along the front edges of the cylinder, which are essentially of opposite nature to that of the upstream vortices (Fig. 10). These vortices gain momentum with streamwise distance and later become the dominant streamwise vortices. Due to the presence of strong transverse flow in the near wake, the streamwise extended vortices issuing from the two lateral sides of the cylinder (which usually possess vorticities of opposite sign) are seen to become compressed and move closer at a downstream location, and while interacting with each other they are observed to get annihilated due to vorticity cross cancellation. Such vorticity cancellation causes local vanishing of the near-wall wake at about three cylinder diameters downstream. With temporal evolution the downstream wake interaction process continued to vary with time and, as a consequence, the location of near-wall wake disappearance was also affected. Interestingly, the location of wake disappearance in all the cases investigated (e.g., flow with different Reynolds number and at different times) was seen to remain closely associated with the local contraction of the wake and the convergence of the instantaneous streamlines on both sides of the downstream saddles (e.g., Figs. 4 and 5). Moreover, after local disappearance of the wake, the nature of the shear layer eruption pattern changed from the upstream monopolar to downstream dipolar form (Figs. 8 and 9). At a higher Reynolds number (Re=500), a very significant temporal distortion in the channel floor flow topology is observed to take place, leading to violent and random eruption of the downstream floor shear layer. Importantly, the near wake in this case became quite compressed and moved closer to the cylinder, and the corresponding process of vorticity cancellation and local wake disappearance were observed to take place at a relatively short distance downstream.

ACKNOWLEDGMENTS

This research was financially supported by the Institute of Physics, Academia Sinica, Taipei, Taiwan, and the National Science Council, R.O.C., Grant No. NSC 90-2611-E-001-002.

[1] C. J. Baker, J. Fluid Mech. **95**, 347 (1979).
[2] P. J. Mason and R. I. Sykes, J. Fluid Mech. **91**, 433 (1979).
[3] J. C. R. Hunt and W. H. Snyder, J. Fluid Mech. **96**, 671 (1980).
[4] A. W. Thomas, Phys. Fluids **30**, 283 (1987).
[5] C. V. Seal, C. R. Smith, O. Akin, and D. Rockwell, J. Fluid Mech. **286**, 117 (1995).
[6] C. V. Seal and C. R. Smith, J. Fluid Mech. **394**, 193 (1999).
[7] P. J. Mason and B. R. Morton, J. Fluid Mech. **175**, 247 (1987).
[8] J. F. Keffer, J. Fluid Mech. **22**, 135 (1965).
[9] C. J. Elliot and A. A. Townsend, J. Fluid Mech. **113**, 433 (1981).
[10] J. C. R. Hunt and I. Eames, J. Fluid Mech. **457**, 111 (2002).
[11] N. J. Cook, B. H. Coulson, and W. McKay, J. Indust. Aerodyn. **2**, 289 (1978).
[12] G. J. Jenkins, P. J. Mason, W. H. Moores, and R. I. Sykes, Q. J. R. Meteorol. Soc. **107**, 833 (1981).
[13] K. B. M. Q. Zaman, M. F. Reeder, and M. Samimy, Phys. Fluids **6**, 778 (1994).
[14] K. B. M. Q. Zaman, J. Fluid Mech. **316**, 1 (1996).
[15] A. Sau, Phys. Fluids **11**, 3003 (1999).
[16] A. Sau, Phys. Fluids **14**, 3280 (2002).
[17] R. M. Kelso and A. J. Smits, Phys. Fluids **7**, 153 (1995).
[18] A. Sau, T. W. Sheu, R. Hwang, and W. C. Yang (unpublished).
[19] T. F. Fric and A. Roshko, J. Fluid Mech. **279**, 1 (1994).
[20] R. M. Kelso, T. T. Lim, and A. E. Perry, J. Fluid Mech. **306**, 111 (1996).
[21] F. M. White, *Viscous Fluid Flow*, 2nd ed. (McGraw-Hill, New York, 1991).
[22] F. H. Harlow and J. E. Welch, Phys. Fluids **8**, 2182 (1965).
[23] Y.-F. Peng, Y-H. Shiau, and R. Hwang, Comput. Fluids **32**, 337 (2003).
[24] T. P. Chiang, T. W. Sheu, R. Hwang, and A. Sau, Phys. Rev. E **65**, 016306 (2002).
[25] J. C. R. Hunt, C. J. Abell, J. A. Peterka, and H. Woo, J. Fluid Mech. **86**, 179 (1978).
[26] J. G. Wissink, Int. J. Numer. Methods Fluids **25**, 51 (1997).
[27] L. L. Yuan, R. L. Street, and J. H. Ferziger, J. Fluid Mech. **379**, 71 (1999).
[28] J. Counihan, J. C. R. Hunt, and P. S. Jackson, J. Fluid Mech. **64**, 529 (1974).
[29] J. M. Wallace and J. L. Balint, Videotape, Turbulence Laboratory, University of Maryland, 1990 (unpublished).